STUDY OF COPPER-NICKEL SYSTEMS USING MAGNETIC QUARTZ CRYSTAL MICROBALANCE

A Thesis
Presented to
The Academic Faculty

By

Kevin Christopher Vavra

In Partial Fulfillment
Of the Requirements for the Degree
Bachelor of Science in Chemistry and Biochemistry

Georgia Institute of Technology

May 2010

Study of Copper-Nickel Systems Using Magnetic Quartz Crystal Microbalance

Approved by:

Dr. Jiří Janata
School of Chemistry and Biochemistry
Georgia Institute of Technology

Dr. Mira Josowicz
School of Chemistry and Biochemistry
Georgia Institute of Technology

Dr. Carrie Shepler
School of Chemistry and Biochemistry
Georgia Institute of Technology

Date Approved: May 07, 2010

TABLE OF CONTENTS

LIST OF TABLES

LIST OF FIGURES

Study of Copper-Nickel Systems Using Magnetic Quartz Crystal Microbalance

Kevin C. Vavra, George Y. Yu, Mira Josowicz, and Jiří Janata
School of Chemistry and Biochemistry, Georgia Institute of Technology, Atlanta, Georgia 30332-0400

It is known that copper and nickel deposited at specific ratios results in alloys that exhibit magnetic properties. The objective of our study is to prepare the Cu-Ni alloys with different magnetic properties and investigate the resulting mechanical properties. To this end, thin alloy films were potentiostatically deposited on gold coated 10MHz piezoelectric quartz crystal microbalances (QCM). Selected deposition potentials varying from -850mV to -1300mV yielded alloys containing varying Ni_xCu_y compositions. Additional studies used alternating pulses of applied voltage that yielded definable pulse widths and heights or an alternate bath that allowed for further investigation on the presence of counterions. Magnetic property characterizations of these depositions were performed using the magnetic quartz crystal microbalance (MQCM) instrument. Preliminary results have demonstrated that the resonant frequency does not change during the application of a magnetic field to homogenous layers of paramagnetic or ferromagnetic materials. However, dispersions of Ni in a non-magnetic Cu matrix produced changes in resonant frequency. Such nickel dispersions can be electrochemically fabrication thereby affecting the magnetically induced QCM resonance shift and admittance magnitude.

1. INTRODUCTION

1.1 Background and Significance

Thin films of magnetic materials have unique mechanical and magnetic properties that are different from bulk magnetic materials. These properties are important in microelectromechanical system (MEMS) applications such as switches, actuators, and inductors. Methods for studying mechanical properties such as *magnetostriction, magnetoelasticity, magnetic susceptibility,* and *magneto-mechanical coercivity* of thin films have been previously described[1-5]. However these methods are expensive, difficult to use, and do not provide a full set of information. A new technique called Magnetic Quartz Crystal Microbalance has been previously investigated by George Yu of the Georgia Institute of Technology using conducting films like polyaniline and gold-nickel stacks[6-8]. This method has multiple advantages; (1) it can be operated at zero magnetic field, (2) it accurately determines the mass of the sample, (3) it measures the sample's baseline mechanical properties.

1.2 Piezoelectric Effect and Quartz Crystal Microbalance

Quartz crystal microbalances (QCM) are composed of a thin piezoelectric quartz disc with two electrodes adhered to the opposite sides of the disc. QCMs can be used to determine the mass of a material bound to the electrodes based on the piezoelectric effect, which occurs when an applied electric voltage produces mechanical strain. Application of an alternating electric field causes an acoustic wave to be generated through the quartz crystal. The quartz crystal oscillates best at the frequency, known as the resonant

frequency, based on the mass of material present. The resonant frequency of the crystal decreases with the addition of mass on the electrode surface (Figure 1)[9]. However the reliability of the quartz crystal can be greatly affected by the temperature stability of the crystal, which is determined by the cut of the crystal during its manufacture[10]. The most common cut for quartz crystals is the AT-cut (Figure 2), since the resonant frequency temperature dependence is zero at 25°C[9, 10].

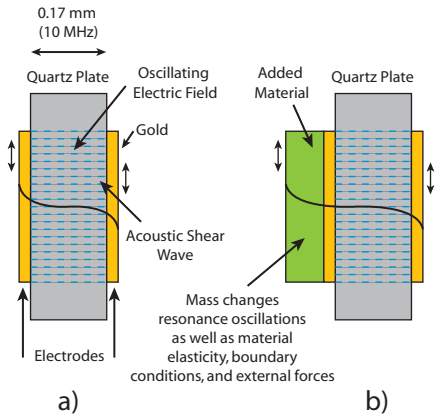

Figure 1: Demonstration of (a) the unloaded QCM operation, and (b) the effect of adding material to the QCM. The addition of mass will change the frequency at which the QCM oscillates. Since the acoustic wave needs to pass through the mass in addition to the quartz, the acoustic properties of the film greatly influence the ability of QCM to measure the material's mass.

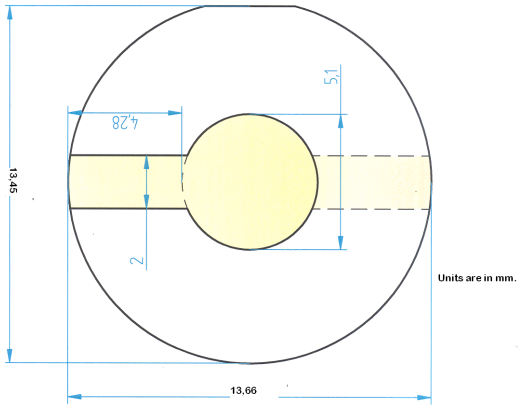

Figure 2: Diagram of AT-cut crystals used in measurements. The electrodes are adhered to both sides of the quartz surface using an adhering layer, usually composed of chromium or titanium. Both electrodes are then connected to an oscillator or network

analyzer in order to determine the resonant frequency of the crystal, which is dependent on the mass present on the QCM electrodes. Figure units are in millimeters.

Günther Sauerbrey first used a quartz crystal to determine small mass changes in a thin rigid film[11]. It eventually became known as a quartz crystal microbalance (QCM), This study established the relationship between the change in resonant frequency and the change in mass deposited on the electrodes of the QCM. The formula for this relation is

$$\Delta f = -\frac{2 f_0^2}{A\sqrt{\bar{c}_{66}\rho_q}}\Delta m \qquad (1)$$

where Δf is the resonant frequency of the crystal, f_0 is the initial resonant frequency, A is the area of the electrode surface, c_{66} is the shear modulus constant (for AT-cut crystals, c_{66} = 2.947x10^{11} g cm^{-1} s^{-2}), ρ_q is the density of quartz (ρ_q = 2.648 g cm^{-3}), and Δm is the change in mass of the film on the electrode surface[8, 12]. Using this equation, which is known as the Sauerbrey equation, to determine a film's mass requires only the resonant frequency and constants pertaining to AT-cut crystals to be known[9]. The ideal relation between frequency and mass is linear; however, using large amounts of material or elastic materials may result in deviations from this behavior[13, 14].

Network analysis proved to be a more powerful technique in monitoring QCM response because the amplitude and phase responses of the crystal can be simultaneously monitored over a spectrum of frequencies[7, 10]. The QCM circuit then follows the Butterworth Van-Dyke (BVD) model and determines the amplitude of admittance or impedance based on BVD equations[7]. Impedance analysis is a great tool to use for studying mechanical properties of films or interfaces between film layers, which are of interest in multilayer stacks[10]. A network analyzer was used in this study, since the

behavior of many different types of thin films with diverse acoustic properties was investigated.

1.3 Magnetic Quartz Crystal Microbalance (MQCM)

Using quartz crystal microbalances to measure the *in situ* magnetic properties of films and materials was first proposed by Yu et al.[6, 7, 15]. Since the mass of the film is not changing during magnetic measurements, the QCM can detect the magnetic response to the applied magnetic field through measurable changes in mechanical properties of the film. The detailed specifications for each part of the MQCM system (Figure 4, in methods) are outlined in previous publications[6, 7, 15], and described in the methods section.

Previous MQCM experiments showed that this technique can be applied to multilayered stacks of electrochemically deposited metals[7, 15]. In or experiments, the electrochemically deposited multilayered arrays were composed of 12, 20, or 28 alternating layers of gold and nickel. As the number of deposited layers increased, the frequency response to the magnetic field measured by the QCM greatly increased. The observed shift in frequency is attributed to the stiffening of the metals in the stack, which causes a decrease in the loss of energy between layers. This decrease in energy loss is predicted to cause the measured shift in resonant frequency[7].

The MQCM technique on multilayer stacks has only been used to measure the properties of thicker layers of nickel and gold deposited from separate solutions. The MQCM method can determine the magnetic properties ofmany for materials. Measuring the magnetic response of different substances will allow for the determination of the

materials that are most sensitive to magnetic fields. This research tested multiple MQCM arrays using alternating layers of a copper alloy as the non-magnetic layer and nickel as the magnetic layer. An additional set of MQCM experiments using single alloys deposited at different temperatures was performed. The use of a copper-nickel alloy requires the use of only one deposition bath; the distinct layers are deposited by alternating the voltages at which deposition occurs. Additional advantages of changing to a copper alloy as the non-magnetic layer could allow for a decrease in acoustic impedance at the interfaces of the layers. A large increase in the frequency observed during the application of the magnetic field will determine if this method can produce sensitive QCM arrays. Determination of the most sensitive materials in MQCM preparation could be used in future applications, such as detecting weak magnetic fields.

1.4 Basic Aspects of Electrochemical Ni-Cu Alloy Film Deposition

Metals, alloys and composite layers can be electrochemically deposited to form single or multi-component films. During deposition, a reduction of ions in the solution takes place when electrons are supplied by an external current source so that the sites for the anodic and cathodic reactions are taking place in separate locations of the system (Figure 3). The electrolytic deposition of binary alloys is a complex process[16]. In order to obtain good alloys, the standard reduction potentials for the components need to be similar. However the standard reduction potentials for copper (Equations 2 and 3) and nickel (Equation 4) versus Standard Hydrogen Electrode are far apart:

$$Cu^{2+} + 2e^{-} \rightarrow Cu^{0} \qquad E° = +0.34V \qquad (2)$$

$$Cu^{2+} + e^{-} \rightarrow Cu^{+} \qquad E° = +0.15V \qquad (3)$$

$$Ni^{2+} + 2e^{-} \rightarrow Ni^{0} \qquad E° = -0.26V \qquad (4)$$

Alloy deposition with large gaps in standard reduction potentials can be induced by shifting the deposition potential of the nobler component, in this case copper, to a more negative value. This can be done by either changing the activity of the discharging ions, adding a complex-forming substance, or by inhibiting the reduction rate of the more noble metal. The influence of additives and changes of electrolysis parameters can greatly influence the production of homogenous deposits without dendritic formations[17]. Changing the current densities of electrodepositions has also been demonstrated as a method to reduce the difference between the deposition potentials[18].

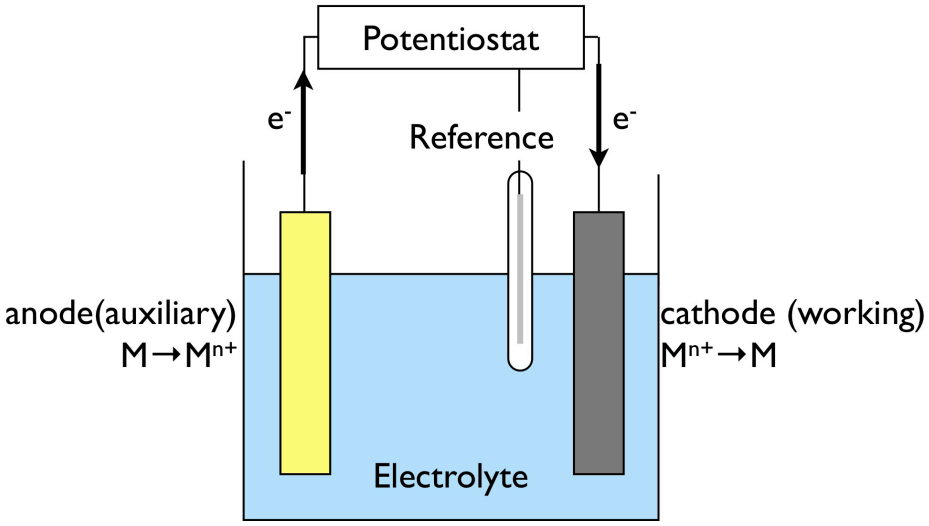

Figure 3: Diagram of typical three electrode electrochemical cell used during deposition. Deposition occurs on the working electrode, which is undergoing reduction. Oxidation occurs at the site of the anode. The DC power supply provides the current needed for deposition to occur.

In this experiment, a copper-nickel alloy was electrochemically deposited by adding copper to a standard Watt's deposition bath[19]. Different ratios of nickel and copper can be deposited based on the voltage applied during deposition. The ratio of copper to nickel was kept at in order to limit the deposition of the more-noble copper during alloy deposition[19]. The high ratio of nickel to copper establishes a mass-transfer

limit on the more noble copper. This allows for both components to be deposited simultaneously from the same solution in order to form an alloy with desired molar ratios of materials.[20] The effects of bath composition and operating conditions during deposition have been studied by Zhou et al.[19]. It has been shown that the composition of the materials was influenced by the component concentrations, bath pH, metal ion ratio, and presence of boric acid.

Furthermore, a multilayered stack containing alternating layers of copper and nickel can be made by depositing nickel from a Watt's bath and then switching to a copper bath. This creates discrete layers of copper and nickel in a Ni/Cu/Ni/Cu/... array. This experiment took a similar approach and attempted to create a multilayered array from the same bath, which contained both copper and nickel. This effect is expected to produce layers composed of Cu-Ni alloys, but each layer can have a different ratio of metals.

2. EXPERIMENTAL

2.1 Materials and Reagents

AT-quartz crystals with a 100Å Ti bonding layer and 1000Å Au electrode area (0.511cm electrode diameter, 1.367 blank diameter, 10MHz crystal) were used in all electrochemical depositions and QCM measurements (International Crystal Manufacturing; Oklahoma City, Oklahoma). Sulfuric and nitric acids, ACS quality, were obtained from BDH Airstar. $NiSO_4 \cdot 6H_2O$ (99.9% purity) was manufactured by J.T. Baker and Co. $NiCl_2$ (99.8% purity), $CuSO_4$ anhydrous (99.8% purity), and boric acid (99.8% purity) were manufactured by Fisher. Deionized water was purified using an ELGA PureLab Ultra water purification system (Veolia Environment S.A.; Paris, France). The EQCM technique was applied to the single potential depositions using a CH 400A potentiostat. For potential pulse depositions required to make multi-layered arrays, a CH 660D electrochemical workstation was used (CH Instruments; Austin, Texas).

2.2 Electrochemical Setup

All depositions were performed in a three-electrode cell using one of the gold electrodes of the QCM as the working electrode. Before mounting, all QCMs were washed with 40% v/v nitric acid, rinsed with deionized water, and then dried under nitrogen gas. The initial resonant frequency was measured and then the QCM was placed in the electrochemical cell. A teflon EQCM cell was used to perform the single potential Cu-Ni alloy depositions, which allowed for additional determination of the changes in

mass. The electrode surface was electrochemically cleaned by cycling in 0.1M sulfuric acid using parameters described in section 3.1.

The reference electrode used in this cell was an Ag / AgCl in 0.1M KCl // 0.1M KNO_3 double junction electrode. A platinum foil auxiliary electrode was used. Electrochemistry using the deposition baths was performed under nitrogen using solutions degassed under vacuum. After each deposition each QCM was washed with deionized water and dried using nitrogen gas. The films were annealed for 24 hours at 50°C before performing the magnetic measurements.

2.3 Copper-Nickel Alloy Bath

Two different baths were used for performing the single potential depositions. The compositions of these solutions are listed in the results section.

The multilayered stacks were made by applying different potentials using the multi-step potential method. Bath I was used for these depositions, which occurred at higher voltages. More information about the parameters tested are listed in section 3.4

2.4 Magnetic Measurements

The system used to perform the magnetic measurements is diagramed in Figure 4. QCM with prepared films are connected to the network analyzer using a sample holding arm that mounts the QCM in a custom-made cell. The sample-holding arm secures the QCM in the center of the cell. The magnetic field is generated by a GMW H-frame model 3473-70 electromagnet powered by a PowerTen R62 60V/100A power supply. The intensity of the actual generated magnetic field is measured by a Lakesore HMMT-6J04-VR/455DSP Hall probe/gaussmeter set. Bias coils are used to counteract

the natural magnetic field of the Earth within the cell, decreasing the initial magnetic field to approximately 0-3G when no current is applied through the primary coils. This allows for accurate measurements of the film's mass and mechanical properties. A computer controls the current applied to the electromagnet and collects the QCM and magnetic field measurements from the network analyzer and Hall probe/gaussmeter, respectively. Further details about this system have been outlined in previous papers[6, 7, 15].

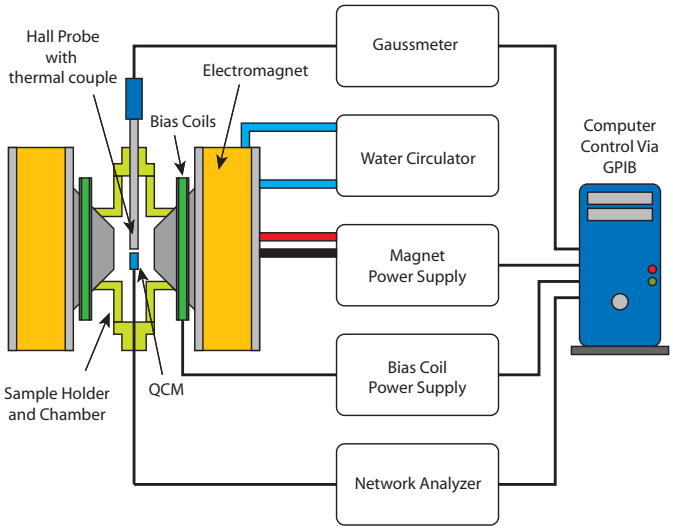

Figure 4: Diagram of the current MQCM system developed and described by Yu et al[7]. QCMs are connected to a network analyzer using a sample holder and then mounted into the sample chamber. A power supply controls the amount of current passing through the electromagnetic coils in order to apply a controlled magnetic field. The network analyzer can then measure the frequency and phase angle data yield to determine any effects caused by a magnetic field. A Hall probe and Gaussmeter are used to measure the actual magnetic field.

All MQCM measurements were performed using a program set to the following parameters: (1) set initial magnetic field to 0kG, (2) perform stepwise increase to 10kG in 1kG increments, (3) perform another step wise decrease to 0kG in 1kG increments. Both the admittance and phase angle traces were collected three times and then averaged to

yield the plot collected at each step in the program. Each film was allowed to rest at zero field before and between measurements for approximately 5 minutes.

2.5 Analysis of MQCM Data

QCM data is collected as admittance and phase angle as a function of frequency over a set window of frequencies during network analysis. This information can provide insight into the effect the magnetic field has on the film since the admittance magnitude and phase angle are changing as the magnetic field is applied. As stated in figure legends, the darker colours for the MQCM plots indicate a higher magnetic field, while lighter colours indicate a lower magnetic field. The information in Figure 5 shows how the information from each trial can be summarized in another format showing how the resonance frequency and admittance magnitude change as a function of the magnetic field. This information is the same for the QCMs that showed a large response to the magnetic field--the admittance magnitude decreases as the magnetic field is applied. This means that the impedance of energy from oscillating the QCM increases. This is attributed to the hardening of material as a response to the magnetic field.

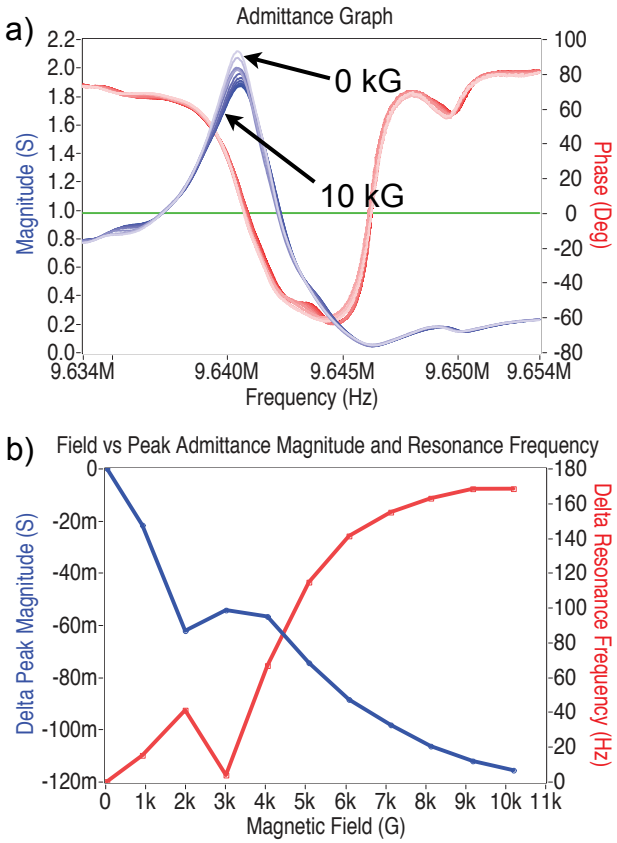

Figure 5: (a) Representative overlay of admittance magnitude and phase angle that can be further analysed to produce the summary presented in (b). The summary shows that the resonant frequency is increasing at the magnetic field is applied, but that the peak magnitude decreases as the field increases.

3. RESULTS

3.1 Electrochemical Cleaning of Gold QCM Electrode

The gold working electrodes were electrochemically cleaned in 0.1M H_2SO_4 using cyclic voltammetry. The cleaning was initiated at 1.2V and cycled to -0.3V at 50mV/s. This was performed until only the oxidation at ~1.2V and reduction at 0.9V of gold was seen. The solution was exchanged with fresh sulfuric acid every three cycles.

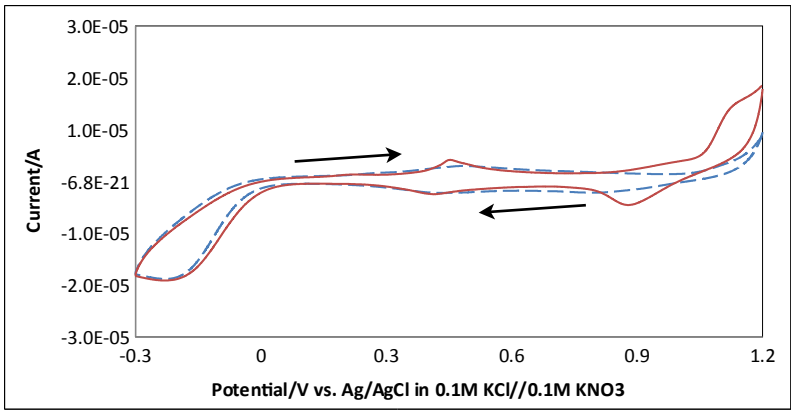

Figure 6: Comparison of the oxidation and reduction of gold in sulfuric acid on a previously cleaned electrode. CVs are recored using a non-degassed solution (solid line) and a degassed solution using nitrogen gas (dashed line).

Figure 6 demonstrates that the degassing of the solution will decrease the area of the peaks that indicate the oxidation of the gold to gold oxide and the reverse reduction. However, most of the electrochemical cleaning procedures were performed with solution that had not been degassed. A crystal was determined to be clean when only one oxidation peak and one reduction peak were visualized in the 0-0.7V range and the CV reached steady state[21] (Figure 7).

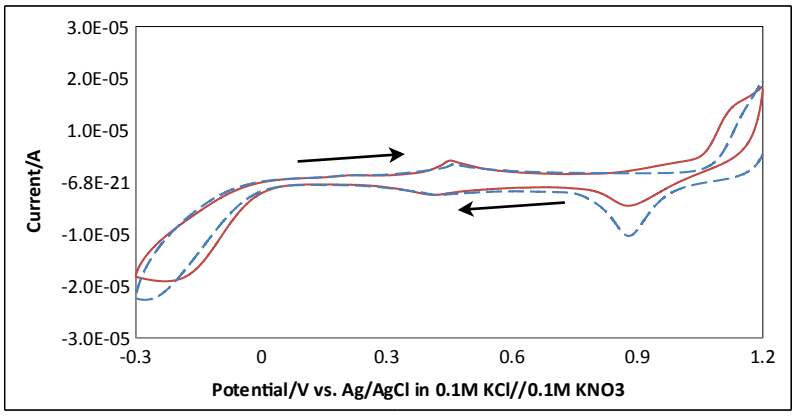

Figure 7: CVs demonstrating the measurable difference between a clean (solid line) and dirty (dashed line) gold electrode in 0.1M H_2SO_4.

3.2 Single Layer Cu-Ni Alloys made with Bath I

First, linear sweep voltammetry was performed on each QCM from open cell potential to the potential at which a nickel-copper alloy will be deposited at 10mV/s in the next step. Deposition of the single layer copper-nickel alloys was performed with limited modification of the Watt's bath previously described by Zhang et al.[19]. The composition of this bath is listed in table 1, and the pH was balanced to equal 4. A CH 400A electrochemical workstation was used for the poteniostatic deposition of the alloy. The resonant frequency change was measured parallel with the current during the QCM conditioning and film deposition.

Table 1: Composition of the modified Watt's bath used for single potential and multipotential depositions. A pH of 4 is confirmed and maintained, if needed, before depositions are performed. The copper-to-nickel ratio is 1 to 200.

Compound	Concentration (mM)	Concentration (g/L, w/v)
H_3BO_3	880	35.92
$NiSO_4 \bullet 6H_2O$	428	111.60
$NiCl_2 \bullet 6H_2O$	78	17.92
$CuSO_4$	3	0.40

The Ni-Cu alloy depositions were performed for both thinner films (approximately 200kHz resonant frequency decrease) and thicker films (correlating to approximately 400kHz resonant frequency change). The thinner film depositions were carried out at -900mV, -1000mV, -1100mV, -1200mV, -1300mV, and -1400mV. The thickness of these layers was controlled by monitoring the resonant frequency and ending the procedure once the resonance frequency reached 200kHz. The thicker film depositions were performed in a smaller potential window but with smaller increments: -900mV, -950mV, -1000mV, -1050mV, -1100mV, -1150mV, -1200mV, -1250mV, and -1300mV. These thicker film depositions were controlled by limited the amount of charge to -1.667C, which calculated to be double the average charge applied to the thinner film depositions.

3.2.1 Linear sweep voltammetry of Ni-Cu deposition

Figure 8 shows the LSV performed from bath I using EQCM. Three peaks can be identified in this LSV: (a) at ~0V the reduction of Cu(II) to Cu(I), (b) ~-0.2V the deposition of Cu(II) to Cu(0), and (c) ~0.75V the deposition of Ni. Peak (b) is accompanied by a decrease in the resonant frequency, indicating a mass increase.

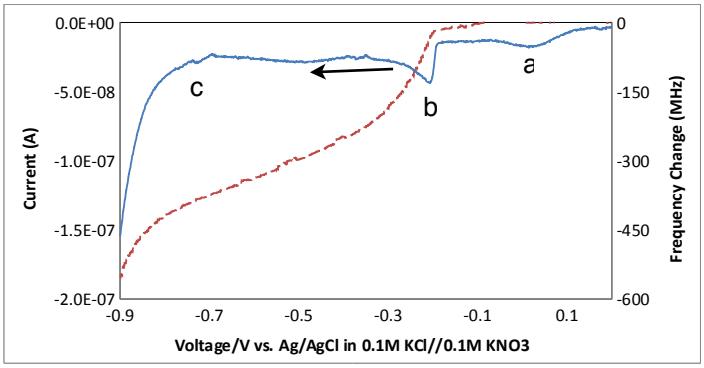

Figure 8: Typical LSV for deposition of Cu-Ni using bath I recorded with 10mV/s (solid line) accompanied by the change in resonant frequency (dashed line).

3.2.2 Potentiostatic film deposition

It is known that the nickel to copper ratios can be changed by controlling the potential at which the deposition is performed[19]. We explored this possibility within the potential window between -900mV and -1400mV. Two sets of films were deposited producing a 200kHz QCM resonant frequency decrease, corresponding to either 180.21µg or 360.42µg of mass, respectively. A typical curve for a potentiostatic deposition at E=-1100mV inside this window is shown in Figure 9. A linear dependence between change in frequency and time suggests that the material was uniformly deposited. The EQCM measurements are limited to changes in frequency, up to ~300kHz.

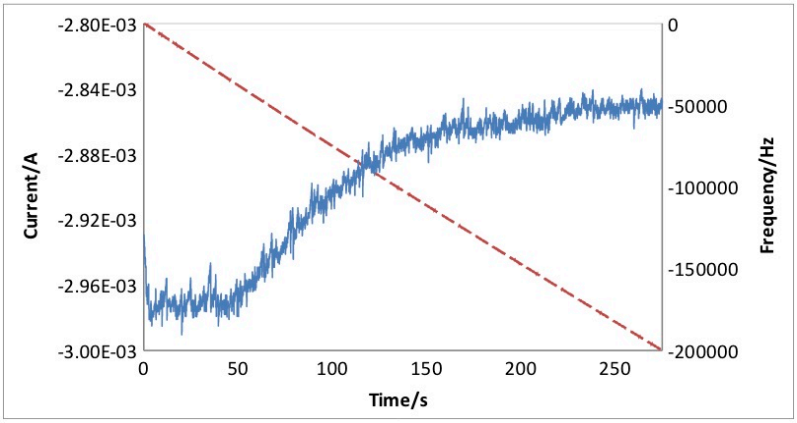

Figure 9: EQCM experiment recorded for the deposition of 180.21µg of Cu-Ni alloy. Changes in current (solid) and frequency (dashed) are depicted 200kHz worth of material was deposited in this experiment..

Figure 10 is an overlay for all amperometry curves obtained during the depositions for the first set of films, each of which caused a resonant frequency decrease of approximately 200kHz. The following deposition potentials were used: (a) -900mV, (b) -1000mV, (c) -1100mV, (d) -1200mV, (e) -1300mV, and (f) -1400mV. Higher deposition currents, and therefore shorter deposition times, were observed when a more negative potential was applied.

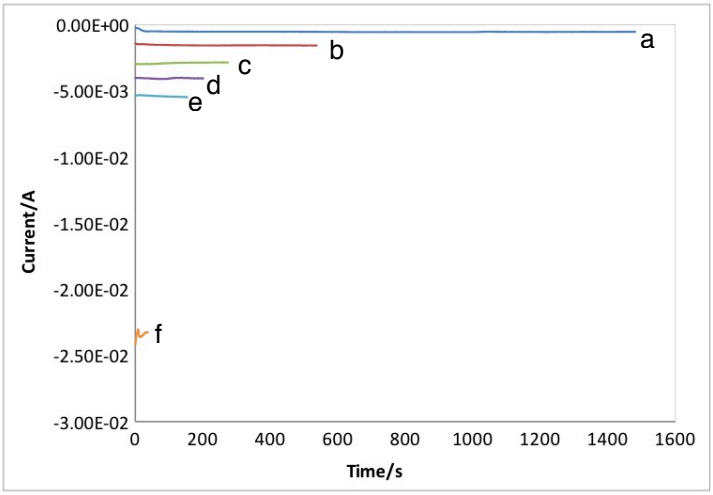

Figure 10: Comparison of potentiostatic depositions performed to produce a 200kHz decrease in resonant frequency at different potentials, which are (a) -900mV, (b) -1000mV, (c) -1100mV, (d) -1200mV, (e) -1300mV, and (f) -1400mV.

A smaller potential window (-900mV to -1300mV) with 50mV increments was used for the depositions of thicker films, which caused a measurable resonant frequency decrease of ~400kHz. Since the EQCM oscillator could not measure frequency changes this large, the experiments were limited by the charge applied, 1.667C, These experiments showed that a larger current was produced as a result of applying a more negative potential. Figure 11 shows the overlaid deposition curves for these films, which have an average thickness of 1.67µm and were performed at (a) -900mV, (b) -950mV, (c) -1000mV, (d) -1050mV, (e) -1100mV, (f) -1150mV, (g) -1200mV, (h) -1250mV, and (i) -1300mV.

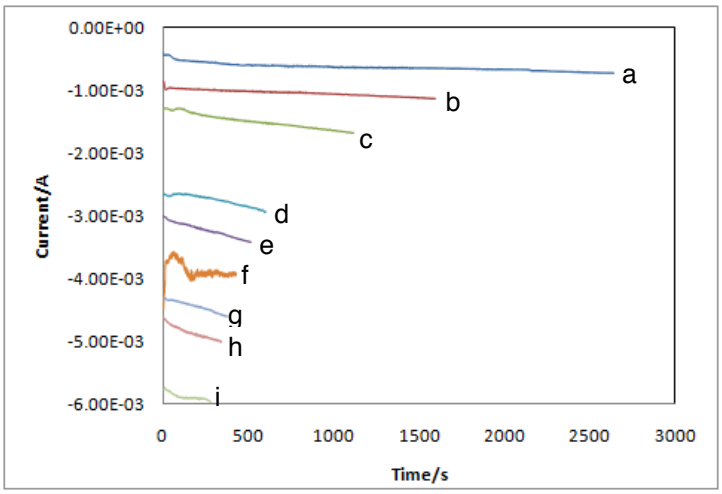

Figure 11: Comparison of potentiostatic depositions for thicker films that cause ~400kHz in resonant frequency shift. The potentials in this figure are (a) -900mV, (b) -950mV, (c) -1000mV, (d) -1050mV, (e) -1100mV, (f) -1150mV, (g) -1200mV, (h) -1250mV, and (i) -1300mV.

The network analyzer used during the magnetic measurements was also used to confirm the initial resonant frequencies and the final resonant frequencies after the film of each crystal dried. Table 2 shows the values for each 400kHz crystal, which were used to calculate the electrochemical plating efficiency in section 4.1.

Table 2: Frequency and mass changes calculated from the Sauerbrey equation for the 400kHz films deposited. However, the actual frequency change for each QCM was not 400kHz, since the EQCM setup abruptly stopped oscillating during mass deposition. The charge applied to each QCM was 1.667C, which is approximately twice the average charge applied to the 200kHz crystals. The average thickness of these depositions is approximately 1.67µm.

Potential (V)	Initial frequency (MHz)	Final frequency (MHz)	Frequency change (kHz)	Mass change (ug)
-0.90	9.9759	9.6372	338.68	306.65
-0.95	9.9766	9.6129	363.77	329.31
-1.00	9.9772	9.6155	361.71	327.41
-1.05	9.9810	9.5833	397.70	359.72
-1.10	9.9747	9.5451	429.56	389.02
-1.15	9.9727	9.5780	394.66	357.56
-1.20	9.9807	9.5432	437.47	395.71
-1.25	9.9774	9.5723	405.08	366.65
-1.30	9.9775	9.5745	402.93	364.70

3.2.3 Magnetic response measured by MQCM

Figures 12-15 depict the plots of the MQCM data collected during the application of the magnetic field, as described in the methods section. The admittance magnitude (Figures 12 and 14) and phase angle (Figures 13 and 15) as a function of frequency were collected to measure a film's response to the magnetic field. The films created at different potentials have markedly different acoustic properties, which accounts for some of the differences at 0 magnetic field. Additionally the films with higher masses, which cause a greater shift in resonant frequency, have shorter and broader peaks in the admittance versus frequency plots.

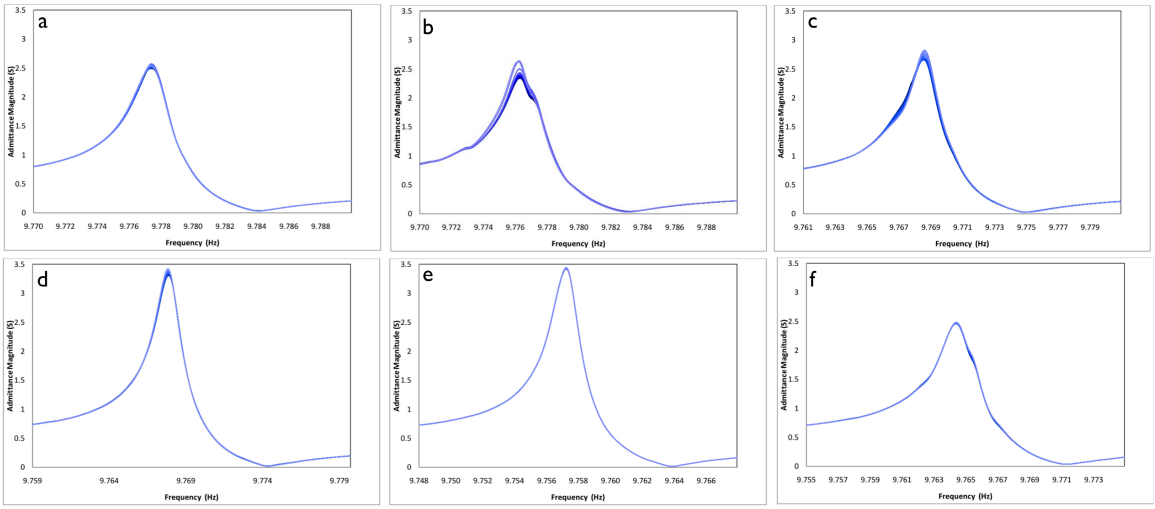

Figure 12: Admittance magnitude vs. frequency measured for the 200kHz MQCM films deposited at (a) -900mV, (b) -1000mV, (c) -1100mV, (d) -1200mV, (e) -1300mV, (f) -1400mV. Each of these plots corresponds with a phase angle vs. frequency diagram in Figure 13. An increasing magnetic field is indicated by a darker line.

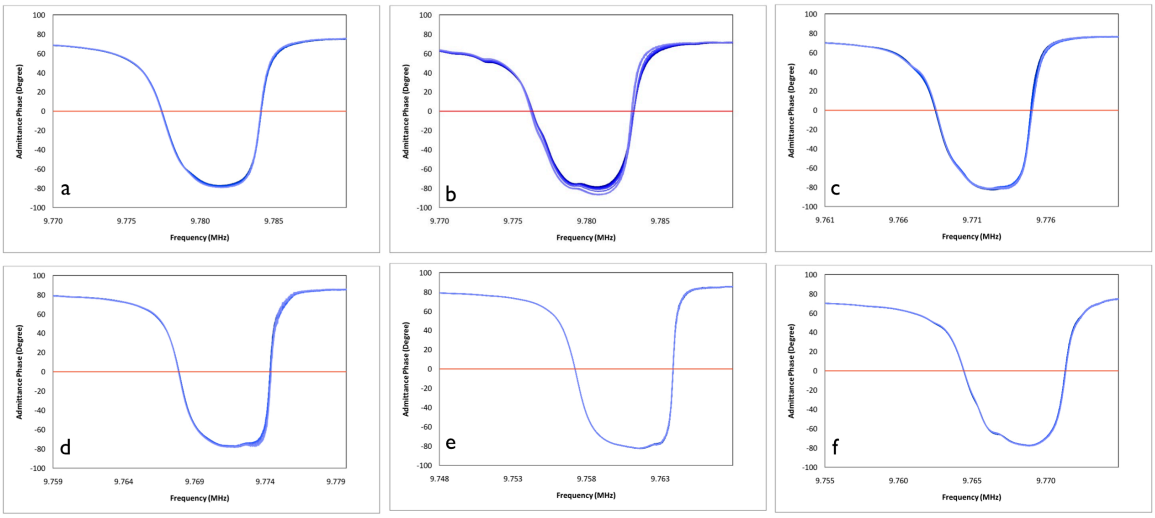

Figure 13: Phase angle vs. frequency measured for the 200kHz MQCM films deposited at (a) -900mV, (b) -1000mV, (c) -1100mV, (d) -1200mV, (e) -1300mV, (f) -1400mV. The 0 phase angle is depicted by the red line in each diagram. The darker blue plots designate an higher applied magnetic field.

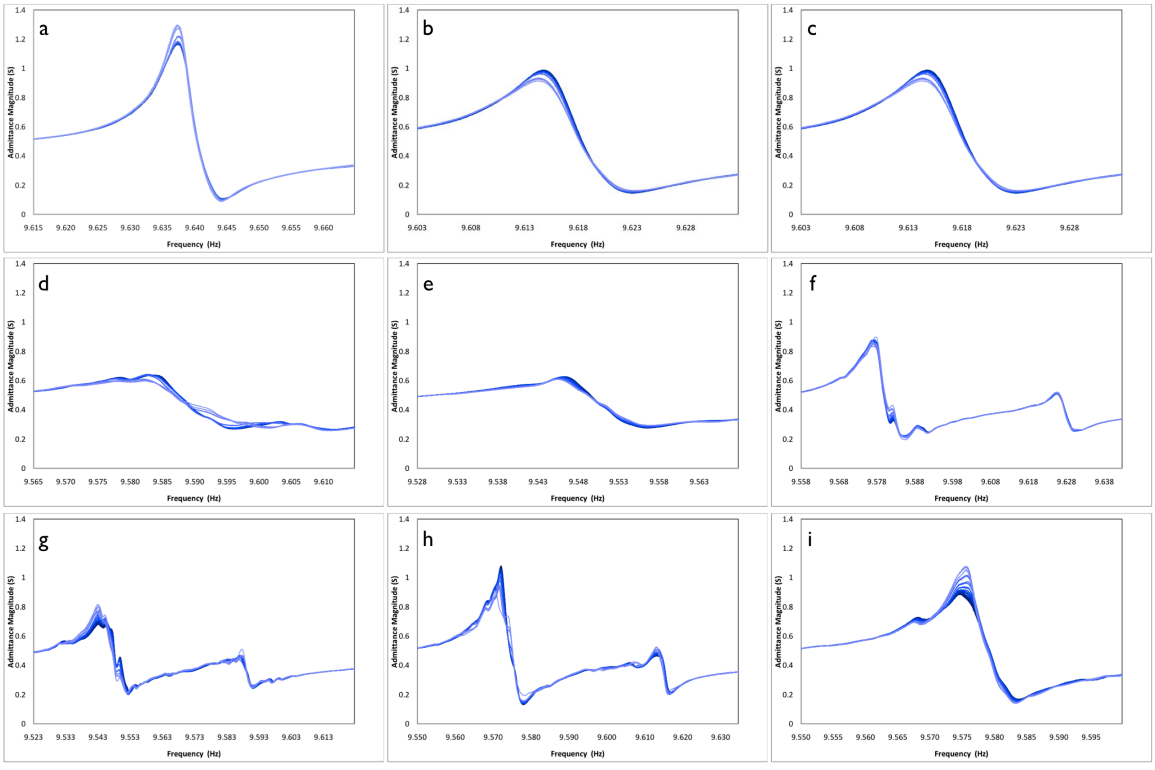

Figure 14: Admittance magnitude vs. frequency measured for the 400kHz MQCM films deposited at (a) -900mV, (b) -950mV, (c) -1000mV, (d) -10500mV, (e) -1100mV, (f) -1150mV, (g) -1200mV, (h) -1250mV, (i) -1300mV. Each of these plots corresponds with a phase angle vs. frequency diagram in Figure 15. The darker plots indicate the a larger value for the applied magnetic field.

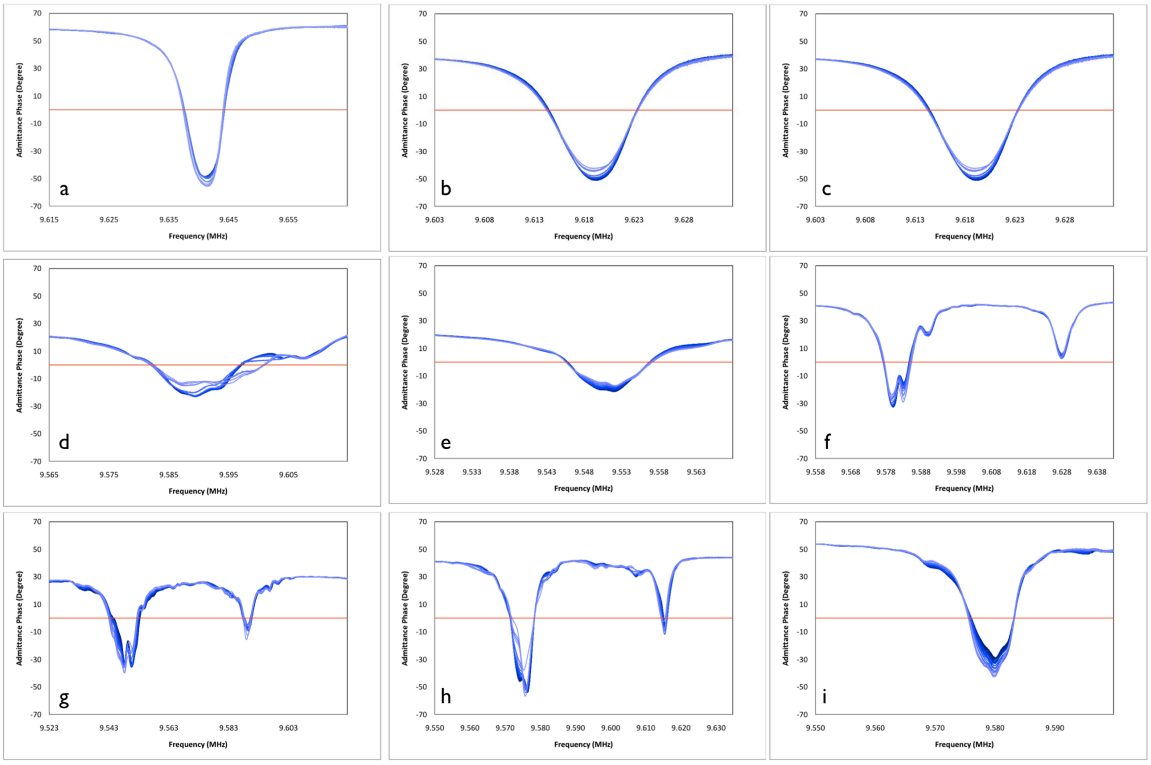

Figure 15: Measured phase angle vs. frequency for the 400kHz MQCM films deposited at (a) -900mV, (b) -950mV, (c) -1000mV, (d) -10500mV, (e) -1100mV, (f) -1150mV, (g) -1200mV, (h) -1250mV, (i) -1300mV. The 0 phase angle is indicated by the red line in each diagram. The darkness of the line indicates the relative strength of the applied magnetic field.

The thicker films demonstrated some unexpected QCM results, such as two admittance or phase angle peaks, which did not appear in the measurements for the thinner films. The meaning of each diagram type and how the interpret the data was described in the methods section 2.3.1. The significance of this data is discussed in further detail in the discussion as well.

3.3 Single Layer Cu-Ni Alloys Made with Bath II

An alternate bath described by Chang et al.[22] was used for additional single potential depositions. Bath II contained a different composition that is listed in Table 3. This bath contains a higher copper-to-nickel ratio (1 to 100) and only sulfate anions. A

linear sweep from +200mV to the deposition potential for each film was performed. The same amount of charge (approximately 1C) of charge was applied at the following voltages during deposition: -750mV, -850mV, -900mV, and -950mV.

Table 3: Composition of bath II used during the single potential depositions described in section 3.3. This bath has a copper-to-nickel ratio of 1 to 100, which is higher than that of bath I.

Compound	Concentration (mM)	Concentration (g/L, w/v)
H_3BO_3	500	30.92
$NiSO_4 \bullet 6H_2O$	1000	203.08
$CuSO_4$	10	1.60

3.3.1 Linear sweep voltammetry of Ni-Cu deposition

Figure 16 shows the LSV deposition carried out using bath II. Linear sweep voltammetry was performed from the open cell potential to the deposition potential (Figure 16) with EQCM to measure the electrochemical activity of this system. This bath did not produce a peak for the reduction of Cu(II) to Cu(I), as seen in the previous bath. This bath only has two reduction peaks: (a) the electrodeposition of copper at ~ -150mV, and (b) nickel deposition at ~ -700mV. The EQCM overlay on the LSV indicates that deposition starts once the Cu deposition begins.

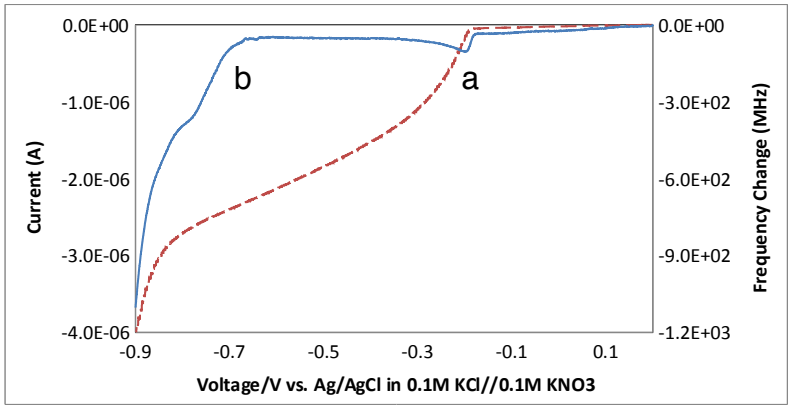

Figure 16: Linear sweep voltammogram (solid line) overlaid with EQCM (dashed line) data from bath II.

3.3.2 Potentiostatic film deposition

The EQCM setup was used to monitor the mass deposited during the deposition using the alternate bath. The charge during the potentiostatic depositions performed between -750mV to -950mV (Figure 17) was limited to approximately 1C, since the QCM would stop oscillating during deposition. This is attributed to the presence of sulfate counter ions, which could potentially cause a film to be rigid[23]. Table 4 shows the mass changes and charges for each deposition.

Table 4: Frequency and mass changes for each deposition, which were calculated from the frequency data obtained from the network analyzer. The charge applied for each deposition is also included, which can be used to demonstrate the effect that both charge and voltage has on deposition.

Potential (V)	Initial frequency (MHz)	Final frequency (MHz)	Frequency change (kHz)	Mass change (ug)	Applied Charge (C)
-0.75	9.9842	9.8022	182.03	164.54	1.2137
-0.85	9.9705	9.7002	270.39	245.08	1
-0.9	9.9750	9.7023	272.71	246.96	1.023
-0.95	9.9717	9.7055	266.20	241.22	1

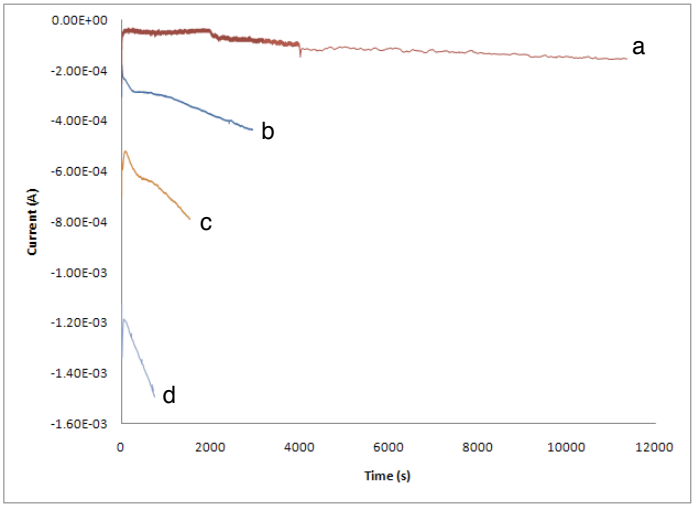

Figure 17: Potentiostatic depositions performed at (a) -750mV, (b) -850mV (c)-900mV (d) -950mV.

The effects of applying more negative voltages during deposition had a similar effect on the current and time during deposition. More negative potentials produced larger currents, yielded shorter deposition times. Table 2 shows the frequency and mass changes calculated from the measurements collected using the network analyzer.

3.2.3 Magnetic response measured by MQCM

The data collected using the network analyzer shows that some films had large acoustic impedance. However some films demonstrated large acoustic admittance, showing that the deposition potential greatly affected the acoustic properties of films made from this bath. The potential window that yielded the films with a measurable response was between -850mV and -900mV, which is a smaller than for bath I.

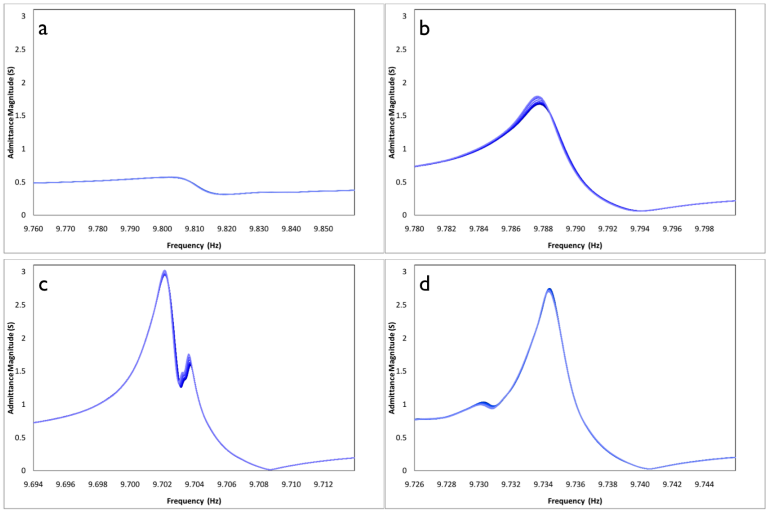

Figure 18: Admittance magnitude vs. frequency measured for films deposited from bath II at (a) -750mV (b) -850mV, (c) -900mV, and (d) -9500mV. The QCM resonant frequency decrease was controlled to be approximately -200kHz. Each of these plots corresponds with a phase angle vs. frequency diagram in Figure 19. The darker plots indicate the a larger value for the applied magnetic field.

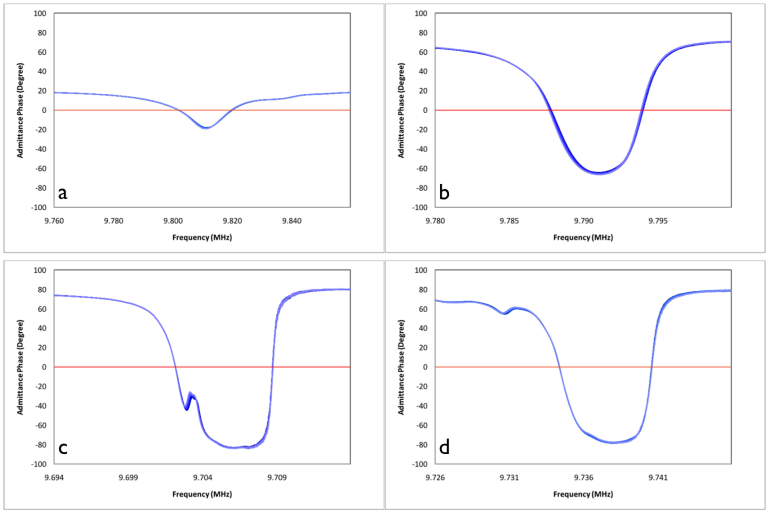

Figure 19: Phase angle vs. frequency measured for the MQCM films deposited from bath II at (a) -750mV, (b) -850mV, (c) -900mV, and (d) -950mV. The 0 phase angle is depicted by the red line in each diagram. The darker blue plots designate an higher applied magnetic field.

3.4 Multilayered Cu-Ni Alloys

Stacks composed of alternating layers of Cu-Ni alloy containing different copper-to-nickel ratios were deposited using an electrochemical workstation programmed using the included multi-potential step method, which would alternate the applied voltage. Composition of the Ni-Cu alloys was determined by alternating the potential between -1.4V (for τ_{low}=0.27 seconds) and -1.6V (for τ_{high}=0.068 seconds) for 500 repetitions. Changing the τ, the time length over which the potential is applied, would deposit thicker or thinner layers of each alloy.

3.4.1 Deposition of Ni-Cu alloys by alternating deposition potential

The multilayered Ni-Cu alloy arrays were deposited with different τ_{low} values for the lower potential step at -1.4V, using $0.25\tau_{low}$, $0.5\tau_{low}$, $1\tau_{low}$, $2\tau_{low}$, and $3\tau_{low}$. The deposition curves indicate the same amount of current being applied though all trials (Figure 20), despite the difference in pulse widths when viewed over a shorter period of

time (Figure 21). The difference between these two potential steps can be observed in Figure 21, which shows a current change every cycle. The more negative potential yields a more negative current, which is why extending τ_{low} causes a measurable increase in the duration of the less negative current.

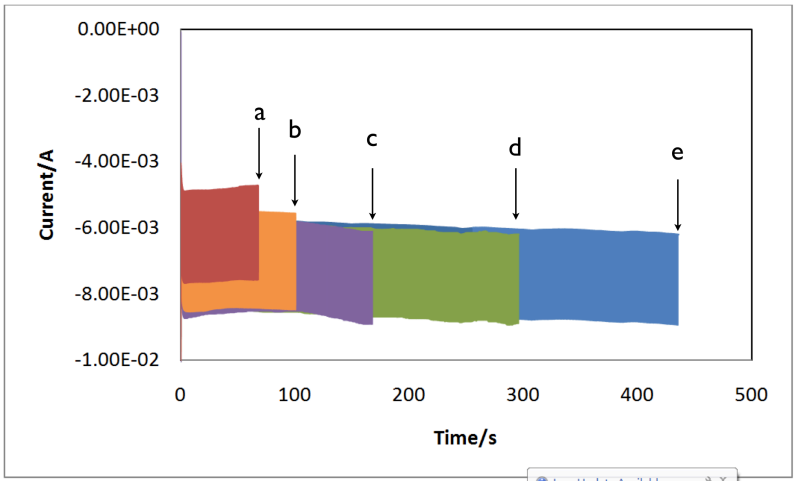

Figure 20: Current vs. time for multilayer alloy depositions ending at the marks (a) 0.25τ, (b) 0.5τ, (c) 1τ, (d) 2τ, and (e) 3τ. The number of deposition cycles were 500 cycles of applying -1.6V and -1.4V. The current range for these depositions was stable across all trials.

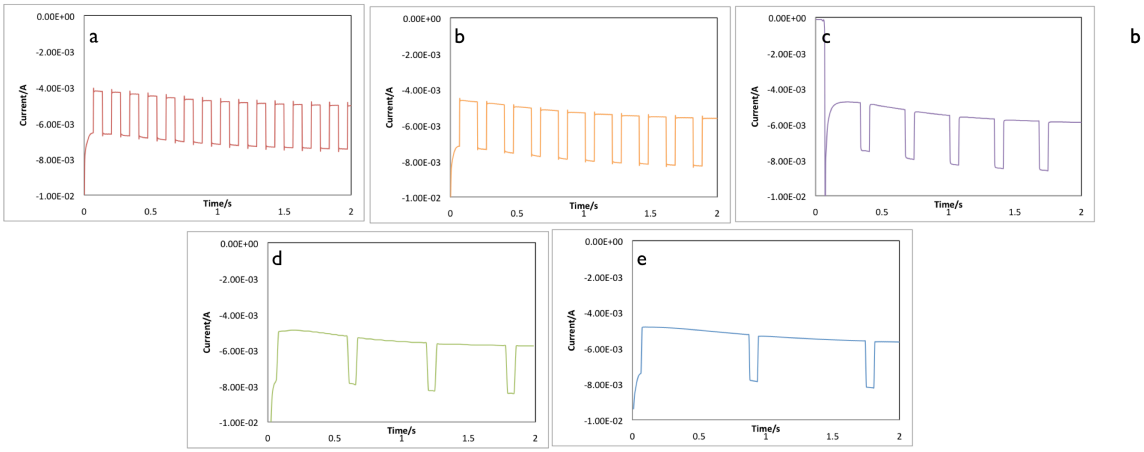

Figure 21: Individual current vs. time plots for the depositions for (a) 0.25τ, (b) 0.5τ, (c) 1τ, (d) 2τ, and (e) 3τ. These curves illustrate the changes in current produced by alternating the applied between two negative potentials.

Table 5: Frequency and mass changes calculated from the measured resonant frequencies before and after deposition using the network analyzer. The applied charge is also present to show that the longer pulse widths were associated with a greater deposition of mass and a larger amount of charge.

Pulse width	initial freq (MHz)	final freq (MHz)	Frequency Change (kHz)	mass change (ug)	Applied Charge (C)
3τ	9.9850	9.2455	739.51	668.34	-2.6838
2τ	9.9850	9.4771	507.92	459.03	-1.8566
1τ	9.9784	9.6761	302.28	273.56	-1.0477
0.5τ	9.9700	9.7761	193.89	175.76	-0.66396
0.25τ	9.9710	9.9613	9.76	8.85	-0.42242

3.4.2 Magnetic response of multilayered arrays

Despite the large amounts of charge and mass deposited on the QCM electrodes, the material deposited did not yield large decreases in admittance magnitude. This allowed for clear measurements to be performed during the application of the magnetic field. Figures 22 and 23 show the admittance versus frequency and phase angle versus frequency, respectively.

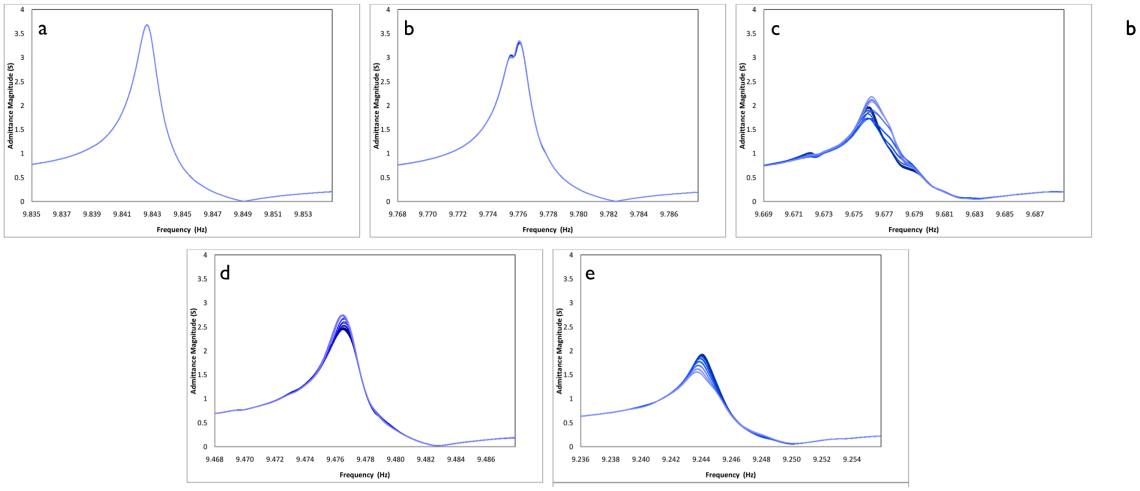

Figure 22: Admittance vs. resonant frequency during the stepwise application of a magnetic field up to 10kG. The pulse widths for these depositions were (a) $0.25\tau_{low}$, (b) $0.5\tau_{low}$, (c) $1\tau_{low}$, (d) $2\tau_{low}$, and (e) $3\tau_{low}$. The darkness of the line represents the relative magnitude of the applied magnetic field--the darker the line, the higher larger the field magnitude.

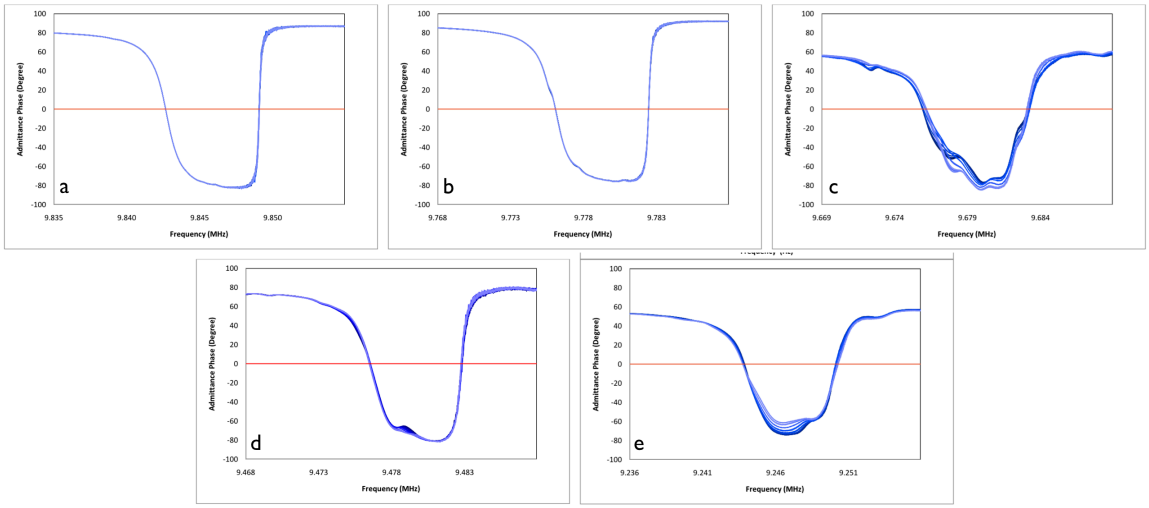

Figure 23: Phase angle vs. resonant frequency for the same measurements performed in Figure 22 for films deposited using pulse widths of (a) $0.25\tau_{low}$, (b) $0.5\tau_{low}$, (c) $1\tau_{low}$, (d) $2\tau_{low}$, and (e) $3\tau_{low}$. The field magnitude is depicted by the darkness of the blue plot, and the red line indicates the location of the 0 phase angle.

4. DISCUSSION AND CONCLUSIONS

4.1 Electrochemical Plating Efficiency

4.1.1 Calculation of alloy deposition efficiency

The mass deposited from an electrochemical procedure can be calculated using the following formula:

$$m = Q * k = Q * \left(\frac{M}{F * z} \right) \tag{5}$$

where Q is the charge in Coulombs, k, is the electrochemical equivalent for the species:

$$k = \frac{M}{F * z} \tag{6}$$

F is Faraday's constant (96485C/mol), M is the molecular weight of the species, and z is the number of involved electrons. However the co-deposition of two or more metals to form an alloy requires further consideration. The total mass deposited in our two component system with nickel and copper can be expressed as the sum of the mass for each component:

$$m_{Tot} = m_{Ni} + m_{Cu} \tag{7}$$

A mole fraction in this system is defined for nickel as:

$$x_{Ni} = \frac{n_{Ni}}{n_{Ni} + n_{Cu}} \tag{8}$$

The mole fraction of copper can be defined similarly to equation8. By combining the mole fractions of each the components with equation 7, we get:

$$x_{Cu} = \frac{n_{Cu}}{n_{Ni} + n_{Cu}} \tag{9}$$

Using the mole fractions to describe the ratios of each component in terms of the total amount of materials deposited allows us to measure the mass of each deposited component in the film. These individual components can be summed together to give the mass total:

$$m_{Tot} = x_{Ni} * m_{Tot} + x_{Cu} * m_{Tot} \tag{10}$$

Substituting equation 10 into equation 6 yields:

$$m_{Tot} = Q * k_{Ni} x_{Ni} + Q * k_{Cu} x_{Cu} \tag{11}$$

This equation can also be rewritten using sum notation, the result of which matches literature values[24]:

$$m_{Tot} = Q \sum k_i x_i = \frac{Q}{F} \sum \frac{x_i M_i}{n_i} \tag{12}$$

This method of calculating the mass will provide a theoretical mass, while using the Sauerbrey equation (equation 1) provides the actual mass deposited. The electrochemical plating efficiency is known to be equal to:

$$\zeta = \left(\frac{m_{actual}}{m_{theoretical}} \right) \times 100\% \tag{13}$$

This is the formula used to determine the efficiency of deposition performed in each bath at different applied voltages.

4.1.2 Deposition efficiency of bath I

The composition of materials deposited using bath I was previously determined using XPS analysis[19]. The mole ratio for nickel to copper can be used from this data and

applied to formula 8 to obtain the theoretical deposition mass. Table 6 presents the plating efficiencies for the potentials at which the alloy film composition is known. The actual mass was obtained from table 2. This data shows that -1.2V is the potential calculated to yield the most efficient deposition, since applying a lower or higher voltage yields a lower plating efficiency.

Table 6: Theoretical masses and plating efficiencies calculated as described in section 4.1.1. The mole ratios for Ni and Cu were obtained from Zhou et al.[19] and then used to calculate the theoretical masses.

Potential (V)	Actual Mass (ug)	Mole Ratio Cu	Mole Ratio Ni	Theoretical Mass (ug)	Plating Efficiency (ζ)
-1.00	327.41	0.2815	0.7185	518.8	63.11%
-1.10	389.02	0.1694	0.8306	514.1	75.67%
-1.20	395.71	0.1391	0.8609	512.9	77.16%
-1.30	364.70	0.0835	0.9165	510.5	71.44%

4.1.3 Deposition efficiency of bath II

Bath II proved to yield lower plating efficiencies compared to bath I. The actual masses were calculated from table 4, while the copper and nickel mole fractions were obtained from previously obtained X-ray diffraction data[22]. The electroplating efficiency of films deposited using this bath are also described in table 7.

Table 7: Theoretical masses and plating efficiencies calculated for bath II using mole ratios previously described[22]. The applied charge and the mole fractions were used to calculate the theoretical masses for each sample. The theoretical masses and actual masses were then used to calculate the electroplating efficiency using equation 9.

Potential (V)	Actual Mass (ug)	Applied Charge (C)	Cu Mole Fraction	Ni Mole Fraction	Theoretical Mass (µg)	Electroplating Efficiency (ζ)
-0.75	164.54	1.2137	0.35	0.65	521.70	32%
-0.85	245.08	1	0.5	0.5	527.99	46%
-0.9	246.96	1.023	0.65	0.35	534.28	46%
0.95	241.22	1	0.85	0.15	542.66	44%

4.2 Conclusions and Future Work

This project included the studies of many different solutions in order to yield the most stable and reproducible depositions. The results demonstrate that the copper-to-nickel ratio in the bath plays an important role for the formation of nickel domains in the copper matrix. The linear sweep of bath I (Figure 8) reveals two peaks in copper deposition--one peak for the reduction of Cu(II) to Cu(I) and then another peak for the reduction of Cu(I) to Cu(0). However similar tests for bath II (Figure 16) do not show a two-step reduction for divalent copper. This could be one of the causes of the less efficient depositions, since both divalent metal cations are deposited without going to an intermediate state.

The electrochemical efficiencies of depositions from bath I as shown in Table 7 were much higher than those calculated in Table 8 for the alternative, bath II. The discrepancies in electrochemical plating efficiencies between bath I and bath II is assumed to be caused by (a) the differences in electrochemical efficiency during deposition and/or (b) changes of film elasticity. Preliminary attempts to use stripping voltammetry to determine the plating efficiencies were performed by holding the

potential in bath I at + 500mV and determining the charge. At that potential, copper was favourably dissolved, and could be monitored by the current produced until it reached a set minimum[22]. Furthermore we propose future characterization of these films using X-ray diffraction (XRD), X-ray photoelectron spectroscopy (XPS), and scanning electron microscopy (SEM). These techniques will provide information on the crystallographic lattice structure, atomic copper-to-nickel ratio at the surface, and morphological features of each deposit.

In summary, this work has shown that either high or low potentials provide the largest magnetic response. These potentials have previously yielded films with a large difference in the molar ratio of the two components, which would cause domains of the low component. This would induce an interrupted matrix of the higher component, which is a proposed cause of the large magnetic response. As stated earlier, changing the composition of the bath changes the domain, size, and mechanical properties of the films. These all influence the performance of the MQCM. Performing additional studies on these materials will provide both more information on the magnetic properties of the Cu-Ni alloy and a better understanding of the MQCM system.

5. REFERENCES

1. M. Inoue, Y. Tsuboi, N. Yokokawa and T. Fujii, IEEE Trans. Magn. **26** (5), 1465-1467 (1990).
2. D. Webb, D. Forester, A. Ganguly and C. Vittoria, IEEE Trans. Magn. **15** (6), 1410-1415 (1979).
3. M. Yamaguchi, K. Hashimoto, H. Kogo and M. Naoe, IEEE Trans. Magn. **16** (5), 916-918 (1980).
4. A. Milewski, J. Samula, L. J. Maksymowicz, J. Wenda, H. Jankowski and A. Kulak, Thin Films **175**, 335-339 (1989).
5. R. F. Wiegert and M. Levy, Journal of Applied Physics **64**, 5411 (1988).
6. G. Y. Yu, W. D. Hunt, M. Josowicz and J. Janata, Review of Scientific Instruments **78** (6), 065111/065111-065111/065116 (2007).
7. G. Y. Yu and J. Janata, Journal of Applied Physics **104** (4), 043908/043901-043908/043906 (2008).
8. G. Y. Yu and J. Janata, Anal. Chem. (Washington, DC, U. S.) **80** (8), 2751-2755 (2008).
9. A. L. Smith, Handb. Therm. Anal. Calorim. **5**, 133-169 (2008).
10. R. Lucklum and F. Eichelbaum, Springer Ser. Chem. Sens. Biosens. **5** (Piezoelectric Sensors), 3-47 (2007).
11. G. Sauerbrey, Z. Phys. **155**, 206-222 (1959).
12. A. Janshoff, H.-J. Galla and C. Steinem, Angewandte Chemie, International Edition **39** (22), 4004-4032 (2000).
13. M. V. Voinova, M. Jonson and B. Kasemo, Biosensors & Bioelectronics **17** (10), 835-841 (2002).
14. d. V. Ivnov and A. Yelon, Proceedings - Electrochemical Society **96-9** (New Directions in Electroanalytical Chemistry), 110-121 (1996).
15. G. Y. Yu, K. C. Vavra and J. Janata, presented at the 215th ECS Meeting, San Francisco, California, 2009 (unpublished).
16. H. Liebscher, Zeitschrift fuer Physikalische Chemie (Munich) **208** (1/2), 183-194 (1999).
17. R. Orinakova, A. Turonova, D. Kladekova, M. Galova and R. M. Smith, Journal of Applied Electrochemistry **36** (9), 957-972 (2006).
18. S. K. Ghosh, A. K. Grover, G. K. Dey and M. K. Totlani, Surface and Coatings Technology **126** (1), 48-63 (2000).
19. M. Zhou, N. Myung, X. Chen and K. Rajeshwar, Journal of Electroanalytical Chemistry **398** (1-2), 5-12 (1995).
20. D. Landolt, Electrochimica Acta **39** (8-9), 1075-1090 (1994).
21. S. J. Xia and V. I. Birss, Journal of Electroanalytical Chemistry (500), 562-573 (2001).
22. J.-K. Chang, S.-H. Hsu, I. W. Sun and W.-T. Tsai, Journal of Physical Chemistry C **112** (5), 1371-1376 (2008).
23. J. Steeb, M. Josowicz and J. Janata, Anal. Chem. (Washington, DC, U. S.) **81** (5), 1976-1981 (2009).

24. H. Ehahoun, C. Gabrielli, M. Keddam, H. Perrot, Y. Cetre and L. Diguet, Journal of the Electrochemical Society **148** (9), B333-B336 (2001).